

Estimating Differential Quantities Using Polynomial Fitting of Osculating Jets

Frédéric Cazals, Marc Pouget

► **To cite this version:**

Frédéric Cazals, Marc Pouget. Estimating Differential Quantities Using Polynomial Fitting of Osculating Jets. L. Kobbelt, P. Schröder, H. Hoppe. Eurographics Symposium on Geometry Processing, Jun 2003, Aachen, Germany. Eurographics, pp.177-187, 2003. <hal-00103047>

HAL Id: hal-00103047

<https://hal.archives-ouvertes.fr/hal-00103047>

Submitted on 2 Mar 2016

HAL is a multi-disciplinary open access archive for the deposit and dissemination of scientific research documents, whether they are published or not. The documents may come from teaching and research institutions in France or abroad, or from public or private research centers.

L'archive ouverte pluridisciplinaire **HAL**, est destinée au dépôt et à la diffusion de documents scientifiques de niveau recherche, publiés ou non, émanant des établissements d'enseignement et de recherche français ou étrangers, des laboratoires publics ou privés.

Estimating Differential Quantities Using Polynomial Fitting of Osculating Jets

F. Cazals[†], and M. Pouget[‡]

Abstract

This paper addresses the pointwise estimation of differential properties of a smooth manifold S —a curve in the plane or a surface in 3D— assuming a point cloud sampled over S is provided. The method consists of fitting the local representation of the manifold using a jet, by either interpolating or approximating. A jet is a truncated Taylor expansion, and the incentive for using jets is that they encode all local geometric quantities—such as normal or curvatures.

On the way to using jets, the question of estimating differential properties is recasted into the more general framework of multivariate interpolation/approximation, a well-studied problem in numerical analysis. On a theoretical perspective, we prove several convergence results when the samples get denser. For curves and surfaces, these results involve asymptotic estimates with convergence rates depending upon the degree of the jet used. For the particular case of curves, an error bound is also derived. To the best of our knowledge, these results are among the first ones providing accurate estimates for differential quantities of order three and more. On the algorithmic side, we solve the interpolation/approximation problem using Vandermonde systems. Experimental results for surfaces of \mathbb{R}^3 are reported. These experiments illustrate the asymptotic convergence results, but also the robustness of the methods on general Computer Graphics models.

Keywords. Meshes, Point Clouds, Differential Geometry, Interpolation, Approximation.

1. Introduction

1.1. Estimating differential quantities

Several applications from Computer Vision, Computer Graphics, Computer Aided Design or Computational Geometry requires estimating local differential quantities. Example such applications are surface segmentation, surface smoothing / denoising, surface reconstruction, shape design. In any case, the input consists of a point cloud or a mesh. Most of the time, estimating first and second order differential quantities, that is the tangent plane and curvature-related quantities, is sufficient. However, applications involving shape analysis^{16,26} require estimating third order differential quantities.

For first to third order differential quantities, a wealth of different estimators can be found in the vast literature of applied geometry²⁴. Most of these are adaptations to the discrete setting of smooth differential geometry results. For example, several definitions of normals, principal directions and curvatures over a mesh can be found in^{32,9}. Ridges of polyhedral surfaces as well as cuspidal edges of the focal sets are computed in³³. Geodesics and discrete versions of the Gauss-Bonnet theorem are considered in²⁵.

A striking fact about estimation of second order differential quantities—using conics and quadrics—is that the classification of Euclidean conics/quadrics is never mentioned. Another prominent feature is that few contributions address the question of the accuracy of these estimates or that of their convergence when the mesh or the sample points get denser. The question of convergence is one prime importance since estimates do not always asymptotically behave as one would expect. For example, it is proved in⁴ that the angular defect of triangulations does not in general provide information on the Gauss curvature of the underlying smooth surface.

The following are provably good approximation results.

[†] INRIA Sophia-Antipolis, 2004 route des Lucioles, F-06902 Sophia-Antipolis; Frederic.Cazals@inria.fr

[‡] INRIA Sophia-Antipolis, 2004 route des Lucioles, F-06902 Sophia-Antipolis; Marc.Pouget@inria.fr

In ¹, an error bound is proved on the normal estimate to a smooth surface sampled according to a criterion involving the skeleton. The surface area of a mesh and its normal vector field versus those of a smooth surface are considered in ²³. Asymptotic estimates for the normal and the Gauss curvature of a sampled surface for several methods are given in ²². In particular, a degree two interpolation is analyzed. Based upon the normal cycle and restricted Delaunay triangulations, an estimate for the second fundamental form of a surface is developed in ⁸.

Deriving provably good differential operators is the goal pursued in this paper. To motivate our guideline and before presenting our contributions, we raise the following question. Second order differential properties for plane curves are almost always investigated using the osculating circle, while principal curvatures of surfaces are almost always computed using osculating paraboloids. Why not osculating parabolas for curves and osculating ellipsoids or hyperboloids for surfaces? Before answering this question and to clarify the presentation, we recall some fundamentals.

1.2. Curves and surfaces, height functions and jets

It is well known ^{10,31} that any regular embedded smooth curve or surface can be locally written as the graph of a univariate or bivariate function with respect to any z direction that does not belong to the tangent space. We shall call such a function a *height function*. Taking an order n Taylor expansion of the height function over a curve yields:

$$f(x) = J_{B,n}(x) + O(x^{n+1}), \quad (1)$$

with

$$J_{B,n}(x) = B_0 + B_1x + B_2x^2 + B_3x^3 + \dots + B_nx^n. \quad (2)$$

Similarly for a surface:

$$f(x,y) = J_{B,n}(x,y) + O(\|(x,y)\|^{n+1}), \quad (3)$$

with

$$J_{B,n}(x,y) = \sum_{k=1}^n H_{B,k}(x,y), \quad H_{B,k}(x,y) = \sum_{j=0}^k B_{k-j,j} x^{k-j} y^j. \quad (4)$$

Borrowing to the jargon of singularity theory ⁵, the truncated Taylor expansion $J_{B,n}(x)$ or $J_{B,n}(x,y)$ is called a degree n jet, or n -jet. Since the differential properties of a n -jet matches those of its defining curve/surface up to order n , the jet is said to have a n order contact with its defining curve or surface. This also accounts for the term *osculating jet* —although osculating was initially meant for 2-jets. The degree n -jet of a curve involves $n + 1$ terms. For a surface, since there are $i + 1$ monomials of degree i , the n -jet involves $N_n = 1 + 2 + \dots + (n + 1) = (n + 1)(n + 2)/2$ terms. Notice that when z direction used is aligned with the normal vector to the curve/surface, one has $B_1 = 0$ or $B_{10} = B_{01} = 0$. The osculating n -jet encloses differential properties of the

curve/surface up to order n , that is any differential quantity of order n can be computed from the n -jet. In particular, the tangent space can be computed from the 1-jet, the curvature related information can be obtained from the 2-jet, locating ridges require coefficients of the 3-jet, and so on. To clarify the presentation, we summarize as follows:

Definition. 1 For a curve or surface:

- given a coordinate system, the *osculating n -jet* is the Taylor expansion of the height function truncated at order n ,
- the osculating n -jet is *principal* if the linear terms vanish in this coordinate system (i.e. the ordinate axis is the normal direction of the manifold),
- an *osculating conic/quadric* is a conic/quadric whose 2-jet matches that of the curve/surface (independently of a given coordinate system),
- an osculating conic/quadric is *degenerate* if it is the graph of its 2-jet,
- an osculating conic/quadric is *principal* if its 2-jet is principal.

Degenerate osculating conics/quadrics are specific curves and surfaces since:

Theorem. 1 ²Chapter 15 There are 9 Euclidean conics and 17 Euclidean quadrics.

Observation. 1 The degenerate osculating conics to a smooth curve are parabola or lines. The degenerate osculating quadrics to a smooth surface are either paraboloids (elliptic, hyperbolic), parabolic cylinders, or planes.

Principal degenerate osculating conics and quadrics are therefore respectively 2 out of 9 conics and 4 out of 17 quadrics. Degenerate stands for the fact that the quadratic forms these conics/quadrics are defined with do not have full ranks.

Principal degenerate osculating conics and quadrics are related to the so-called Monge form of the curve or surface, that is the local Taylor expansion of the curve/surface in the Monge coordinate system. The Monge coordinate system of a curve is defined by its tangent and normal vectors. For a surface, the Monge coordinate system is such that the z axis is aligned with the normal and the x,y axis are aligned with the principal directions. In this particular system, the height function is called the Monge form, and letting k_1, k_2 stand for the principal curvatures, one has —with *hot* standing for *higher order terms*:

$$f(x,y) = \frac{1}{2}(k_1x^2 + k_2y^2) + hot \quad (5)$$

From these observations, the question we ended paragraph 1.1 with can now be answered. By theorem 1 and observation 1, using a general conic/quadric or a principal degenerate one to approximate a curve or a surface does not

make any difference. In both case and up to order two, the local differential properties of the curve/surface, degenerate conic/quadric, or full rank conic/quadric are identical. As an example, consider Figure 1(a,b,c). Figure 1(a) features a curve and its osculating circle. In (b), the osculating circle is replaced by the principal osculating parabola—whose symmetry axis is the normal to C and whose curvature matches that of C . At last, in (c) a general parabola locally approximates C . Its symmetry axis is not aligned with the normal to C .

Summarizing our discussions so far, the rationale for fitting the n -jet of a curve/surface is that this polynomial contains all the differential information up to order n .

1.3. Interpolation, approximation and related variations

Our methodology to retrieve differential quantities consists of fitting the osculating jet. The following variations need to be discussed in order to state our contributions precisely. The case of curves and surfaces being tantamount, our description focuses on surfaces. Assume we are given a set of N points $p_i(x_i, y_i, z_i), i = 1, \dots, N$ in the neighborhood of a given point p on the surface processed. Point p itself may or may not be one of the N samples, and one can assume without loss of generality that p is located at the origin of the coordinate system used.

Interpolation versus approximation. Interpolating consists of finding a polynomial that fits exactly a set of data points. In our case and following Equation (3), let B index a coefficient of the jet of the surface, and A index a coefficient of the jet sought. We aim at finding a n -jet $J_{A,n}$ such that $\forall i = 1, \dots, N$

$$f(x_i, y_i) = J_{B,n}(x_i, y_i) + O(\|(x_i, y_i)\|^{n+1}) = J_{A,n}(x_i, y_i). \quad (6)$$

As a mnemonic, the reader may want to remind that index A stands for the *Answer* to the fitting problem.

Approximation, on the other hand, gives up on exactness, that is the graph of the jet sought may not contain the sample points. We shall focus on *least-square* approximation, which consists of minimizing the sum of the square errors between the value of the jet and that of the function. The quantity to be minimized is therefore

$$\sum_{i=1}^N (J_{A,n}(x_i, y_i) - f(x_i, y_i))^2. \quad (7)$$

The two problems can actually be written in the same matrix form. To see why, let us write the jets in the polynomial basis consisting of monomials $x^i y^j$. Example other basis that could be used are the Bezier-Bernstein basis or the Newton basis. We use the monomials since this basis is convenient for the asymptotic analysis but also the design of effective

algorithms. Denote A be the N_n -vector of the coefficients of the jet sought, that is

$$A = (A_{0,0}, A_{1,0}, A_{0,1}, \dots, A_{0,n})^t.$$

Denote B the N -vector of the ordinates, i.e. with $z_i = f(x_i, y_i)$,

$$B = (z_1, z_2, \dots, z_N)^t = (J_{B,n}(x_i, y_i) + O(\|(x_i, y_i)\|^{n+1}))_{i=1, \dots, N}.$$

Equations (6) and (7) yield the following $N \times N_n$ Vandermonde matrix

$$M = (1, x_i, y_i, x_i^2, \dots, x_i y_i^{n-1}, y_i^n)_{i=1, \dots, N}. \quad (8)$$

For the interpolation case, the number of points matches the number of parameters, so that matrix M is square and Eq. (6) can be written as $MA = B$. For the approximation case, M is a rectangular $N \times N_n$ matrix, and Eq. (7) is summarized as $\min \|MA - B\|_2$.

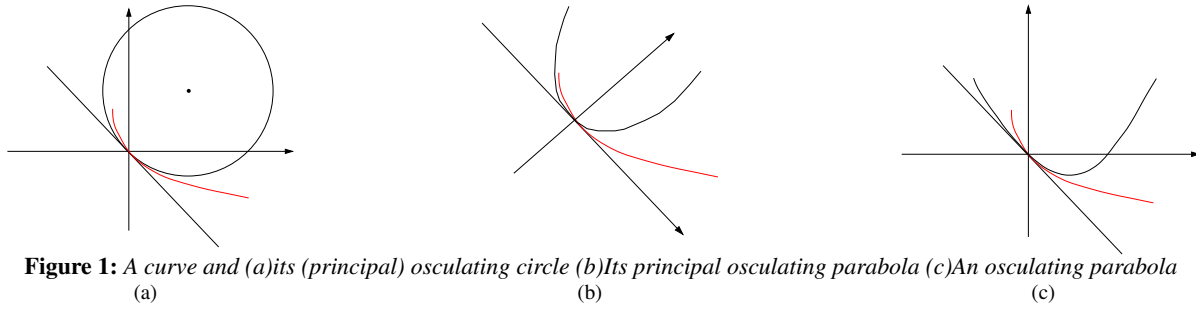
Choosing between interpolation and approximation depends upon the problem tackled. For noisy datasets, approximation is the method of choice. Otherwise, the alternative depends of the relative values of the number of model parameters versus the number of available points. If the two match one-another, a natural choice is interpolation. In any case, fitting yields a linear system, so that numerical issues arise. Facing these difficulties is the topic of section 2.

Mesh or meshless methods. An important difference between local geometry estimation algorithms is whether or not they require some topological information—typically the connectivity of a mesh. Mesh-based methods are usually faster. Meshless techniques are more general and better suited for noisy datasets. A difficulty of the latter methods, however, is to select the relevant points used to perform the estimates. While one can always resort to heuristics of the k -nearest-neighbors type, user defined parameters should be avoided. This issue is addressed in section 5.

One or two stages methods. Fitting a 2-jet requires estimating the tangent plane and the curvature related information. These steps can be carried out sequentially or simultaneously. Following the guideline of ²⁷, most of the methods already mentioned proceed sequentially. The provably good algorithm we propose proceeds simultaneously. Along its analysis, we also provide theoretical results on the accuracy of sequential methods¹³.

1.4. Contributions

Jet interpolation and approximation. Consider Eqs. (6) and (7). We expect $J_{A,n}$ and $J_{B,n}$ to be equivalent in some sense. To specify this, we shall study the convergence properties of the coefficients of $J_{A,n}$ when the points p_i s converge to p . More precisely, assume that the coordinates of the p_i s are given by $p_i(x_i = a_i h, y_i = b_i h, z_i = f(x_i, y_i))$. Parameters a_i and b_i are arbitrary real numbers, while h specifies that



the p_i s uniformly tend to the origin. We actually expect

$$A_{ij} = B_{ij} + O(r(h)).$$

Function $r(h)$ describes the convergence rate or the precision of the fitting, and the main contribution of this paper is to quantify $r(h)$ for interpolation and approximation methods. As we shall see, interpolation or approximation of the same degree yield the same convergence rate. The difficulties posed are also similar and are essentially to deal with singular matrices.

Relationship to previous theoretical contributions. The theoretical results we are aware of are twofold. First, in ²²Lemma 4.1, a degree two interpolation is used and analyzed. We deal with jets or arbitrary degree, for interpolation and approximation. Second, convergence results on the coefficients of the Lagrange interpolation polynomial versus the Taylor expansion of a function are proved in ⁷. Our results match those, but we also analyze the approximation case. Most importantly, we give constructive proofs and develop the corresponding algorithms.

It should be noticed that we are *not* concerned here with the convergence of the Lagrange interpolation polynomial to the height function on a whole given set. This problem requires specific conditions on the function and the position of the points, as illustrated by the Runge divergence phenomena ¹⁹Chapter 2. Therefore, our study is not to be confused with global fitting such as piecewise polynomial fitting encountered in CAD.

Due to the lack of space, the reader is referred to ⁶ for the proofs.

2. Interpolation, approximation, numerical issues

In this section, we recall the fundamentals of the fitting methods used, namely interpolation and approximation, together with the numerical issues arising from the resolutions.

2.1. Interpolation

The interpolation fitting is based upon the Lagrange interpolation, that is the construction of a polynomial constrained

to fit a set of data points. Although this problem is classical for the univariate case, the multivariate case is still an active research field from both the theoretical and computational points of view. We briefly review the univariate and multivariate basics of Lagrange interpolation.

Univariate Lagrange interpolation. Let $X = \{x_0, \dots, x_n\}$ be $n + 1$ distinct real values, the so-called *nodes*. Then, for any real function f , there is a unique polynomial P of degree n so that $P(x_i) = f(x_i), \forall i = 0, \dots, n$. Polynomial P is called the *Lagrange interpolation polynomial* of f at the nodes X . For any choice of distinct nodes, this polynomial exists and is unique, and in that case the Lagrange interpolation is said to be *poised*.

Multivariate Lagrange interpolation. Consider now the following bivariate problem. Let Π_n be the subspace of bivariate polynomials of total degree equal or less than n , whose dimension is $N_n = \binom{n+2}{n}$, and let $X = \{x_1, \dots, x_N\}$ consist of $N = N_n$ values in \mathbb{R}^2 called nodes. (Notice that N is exactly the number of monomials found in the jet of Equation 3.) The Lagrange interpolation problem is said to be poised for X if for any function $f : \mathbb{R}^2 \rightarrow \mathbb{R}$, there exists a unique polynomial P in Π_n so that $P(x_i) = f(x_i), \forall i = 1, \dots, N$. It is intuitive and well known that this problem is poised iff the set of nodes X is not a subset of any algebraic curve of degree at most n , or equivalently the Vandermonde determinant formed by the interpolation equations does not vanish. As noticed in ²⁹, the set of nodes for which the problem is not poised has measure zero, hence it is almost always poised.

However let us illustrate non-poised cases and almost non-poised or degenerate ones. Consider the two quadrics $q_1(x, y) = 2x + x^2 - y^2$ and $q_2(x, y) = x^2 + y^2$, whose intersection curve I projects in the (x, y) plane to the conic $C(x, y) = 0$ with $C(x, y) = x - y^2$ —Figure 2. If one tries to interpolate a height function using points on I , uniqueness of the interpolant is not achieved since any quadric in the pencil of q_1 and q_2 goes through I . A similar example featuring the four one-ring and one two-ring neighbors of a point p is depicted on figure 3. Notice that being able to figure out such configurations is rather a strength than a weakness of the method since a surface is sought and, the amount of infor-

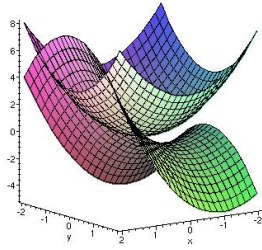


Figure 2: Two quadrics whose intersection curve I projects onto the parabola $C : x = y^2$. Interpolation points located on I do not uniquely define an interpolating height function.

mation available does not determine uniquely this surface. A first fundamental difference between the univariate and multivariate cases is therefore the critical issue of choosing nodes so that the interpolation is poised.

In the particular case where the points lies on a regular square grid of the plane, the geometry of the configuration leads to the following remarks. On one hand, a non-poised degree n interpolation occurs if the points lies on n lines, since they define an algebraic curve of degree n . One the other hand, triangular lattices yield poised problems for every degree. These results and further extensions can be found in ¹² and references therein.

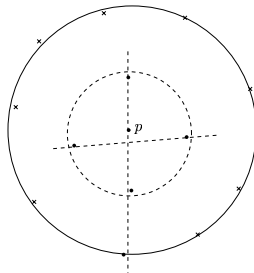


Figure 3: The Kite (almost) degenerate configuration — tangent plane seen from above: the 6 points used for a degree two interpolation are (almost) located on a degenerate conic, that is two intersecting lines.

2.2. Least square approximation

It is well known that the minimization problem of Eq. (7) has a unique solution iff the matrix M is of maximum rank N_n . In that case, the minimum value ρ is called the *residual* of the system, that is $\rho = \min \|MA - B\|_2$. The important issue is again the rank of the matrix M . In terms of the relative values of N versus N_n , using too many points certainly smoothes out geometric features, but also makes rank deficient matrices less likely.

2.3. Numerical Issues

The difficulties of solving linear and least-squares systems consist of dealing with rank-deficient matrices. We now discuss these issues in more detail. Distances between matrices and matrix norms refer to the Euclidean norm.

Singular systems and condition numbers. To quantify degeneracies, we resort to a Singular Value Decomposition (SVD) ¹⁴. Denote $\sigma_n, \dots, \sigma_1$ the singular values of M sorted in decreasing order. It is well known that the least singular value of M is the distance from M to rank deficient matrices. The singular values also characterizes the sensitivity of the problem, that is the way errors on the input data induce errors on the computed solution. Notice that errors refer to the uncertainty attached to the input data and not to the rounding errors inherent to the floating point calculations. In our case, input data are the sample points, so that errors are typically related to the acquisition system —e.g. a laser range scanner.

To quantify the previous arguments, we resort to the *conditioning* or *condition number* of the system ^{14,17}. The conditioning is defined as a magnification factor which relates the afore-mentioned errors by the following rule $\text{Error on solution} = \text{Error on input} \times \text{conditioning}$. Denote

$$\kappa_2(M) = \|M\|_2 \|M^{-1}\|_2 = \sigma_n / \sigma_1$$

the condition number of the matrix M . The conditioning in the two cases are respectively given by

$$\begin{cases} \text{linear square system: } \kappa_2(M), \\ \text{least square system: } \kappa_2(M) + \kappa_2(M)^2 \rho \end{cases} \quad (9)$$

with $\rho = \|MX - B\|_2$ the residual.

The following theorem provides precise error bounds:

Theorem. 2 Suppose X and \tilde{X} are the solutions of the problems

$$\begin{cases} \text{linear square system: } MX = B \text{ and } (M + \Delta M)\tilde{X} = B + \Delta B, \\ \text{least square system: } \min \|MX - B\|_2 \text{ and} \\ \min \|(M + \Delta M)\tilde{X} - (B + \Delta B)\|_2, \end{cases} \quad (10)$$

with ε a positive real value such that $\|\Delta M\|_2 \leq \varepsilon \|M\|_2$, $\|\Delta B\|_2 \leq \varepsilon \|B\|_2$, and $\varepsilon \kappa_2(M) < 1$. Then one has:

$$\frac{\|X - \tilde{X}\|_2}{\|X\|_2} \leq \varepsilon \text{ conditioning.} \quad (11)$$

In practice, if the conditioning is of order 10^a and the relative error on the input is $\varepsilon \approx 10^{-b}$ — with $\varepsilon \kappa_2(M) < 1$, then the relative error on the solution is of order 10^{a-b} .

Pre-conditioning the Vandermonde system. As already discussed, a convenient way to solve Eqs. (6) and (7) consists of using the basis of monomials. One ends up with the Vandermonde matrix of Eq. (8), that can be solved with usual

methods of linear algebra. Unfortunately, Vandermonde systems are known to be ill-conditioned due to the change of magnitude of the terms. We therefore pre-condition so as to improve the condition number. Assuming the x_i s, y_i s are of order h , the pre-conditioning consists of performing a column scaling by dividing each monomial $x_i^k y_i^l$ by h^{k+l} .

The new system is $M'Y = MDY = B$ with D the diagonal matrix $D = (1, h, h, h^2, \dots, h^n, h^n)$, so that the solution A of the original system is $A = DY$. The condition number used in the sequel is precisely $\kappa(M')$. (Notice it has the geometric advantage to be invariant under homothetic transformations of the input points.) Then the accuracy of the result can be estimated a posteriori, and almost degenerate cases highlighted by large conditioning.

Alternatives for the interpolation case. An alternative to the Vandermonde system consists of using the basis of Newton polynomials. Resolution of the system can be done using divided differences²⁸, a numerically accurate yet instable method¹⁷.

3. Surfaces

3.1. Problem addressed

Let S be a surface and p be a point of S . Without loss of generality, we assume p is located at the origin and we aim at investigating differential quantities at p . Consider the height function f given by Equation (3) in any coordinate system whose z axis is not in the tangent plane. We shall interpolate S by a bivariate n -jet $J_{A,n}(x, y)$ whose graph is denoted Q .

The normal to a surface given by Equation (3) is

$$n_S = (-B_{10}, -B_{01}, 1)^t / \sqrt{1 + B_{10}^2 + B_{01}^2}. \quad (12)$$

In order to characterize curvature properties, we resort to the Weingarten map A of the surface also called the shape operator, that is the tangent map of the Gauss map. (Recall that the second fundamental form II and A satisfy $II(v) = \langle A(v), v \rangle$ for any vector v of the tangent space.) The principal curvatures and principal directions are the eigenvalues (eigenvectors) of A , and the reader is referred to¹⁰Section 3.3. If the z axis is aligned with the normal, the linear terms of Equation (3) vanish, and the second fundamental form reduces to the Hessian of the height function. Further simplifications are obtained in the Monge coordinate system, where $I = Id_2$, the Hessian is a diagonal matrix, and the principal curvatures are given by $2B_{20}$ and $2B_{02}$.

3.2. Polynomial fitting of the height function

We begin by an approximation result on the coefficients of the height function. We focus on the convergence rate given by the value of the exponent of parameter h .

Proposition. 1 A poised polynomial interpolation or a polynomial approximation of degree n based upon N points

$p_i(x_i, y_i, z_i)$ whose abscissa are $x_i = O(h), y_i = O(h)$ estimates the coefficients of degree k of the Taylor expansion of f to accuracy $O(h^{n-k+1})$:

$$A_{k-j,j} = B_{k-j,j} + O(h^{n-k+1}) \quad \forall k = 0, \dots, n \quad \forall j = 0, \dots, k.$$

Moreover, if the origin is one of the p_i s, then $A_{0,0} = B_{0,0} = 0$.

Using the previous proposition, the order of accuracy of a differential quantity is linked to the degree of the interpolant and the order of this quantity. More precisely:

Theorem. 3 A polynomial fitting of degree n estimates any k^{th} -order differential quantity to accuracy $O(h^{n-k+1})$. In particular:

- the coefficients of the unit normal vector are estimated with accuracy $O(h^n)$, and so is the angle between the normal and the estimated normal.
- the coefficients of the first, second fundamental form and shape operator are approximated with accuracy $O(h^{n-1})$, and so are the principal curvatures and directions.

The previous theorem generalizes²²Lemma 4.1 where 2-jet interpolations only are studied. The $O(h^n)$ bound on the normal should also be compared to the normal estimate of the normal vector using specific Voronoï centers called poles considered in¹. The error bound proved there is equivalent to 2ε with ε the sampling density of the surface. Setting $h = \varepsilon lfs$ and assuming lfs is bounded from above, the estimation stemming from a polynomial fitting therefore yields more accurate results for the normal, and also provides information on higher order quantities. From an algorithmic perspective, and according to proposition 2, it is sufficient to perform the fitting in any coordinate system.

3.3. Accuracy of the fitting and relationship to the coordinate system

Proposition 1 involves any admissible coordinate system. From a practical standpoint, we would like to perform the fitting in some arbitrary coordinate system, compute the normal and principal directions, and infer the height function in the Monge coordinate system. Notice that this is not completely straightforward since rewriting a height function in a different coordinate system results in an implicit equation for the corresponding surface—we had $z = f(x, y)$, but x, y, z become linear combinations of the new variables x', y', z' . The following proposition shows that calculations can indeed be performed in this order, and that no accuracy is lost along the process. The constructive proof uses the implicit function theorem and is omitted.

Proposition. 2 Let $J_{A,n}$ be the n -jet estimating $J_{B,n}$ in a coordinate system D , and let Q be the surface associated with $J_{A,n}$. Let D' be another coordinate system, $J'_{B,n}$ ($J'_{A,n}$) the n -jet of S (Q) in D' . If $A_{k-j,j} = B_{k-j,j} + O(h^{n-k+1})$, then $A'_{k-j,j} = B'_{k-j,j} + O(h^{n-k+1})$.

3.4. Influence of normal accuracy on higher order estimates

Following the guideline initiated in ²⁷ several algorithms first estimate the normal to the surface and then proceed with Hessian of the height function. We analyze the error incurred by the latter as a function of the accuracy on the former. We denote θ the angle between the normal n_S to the surface and the normal n_Q estimated by the two-stages method. In order to simplify calculations, we assume that n_Q is aligned with the z -axis and n_S is in the (x, z) -plane, so that $f(x, y) = B_{10}x + B_{20}x^2 + B_{11}xy + B_{02}y^2 + O(\|(x, y)\|^3)$, with $B_{10} = -\tan \theta$. Expressed in the same coordinate system, the interpolant—a 2-jet to simplify calculations—reads as $J_{A,2}(x, y) = A_{20}x^2 + A_{11}xy + A_{02}y^2$.

Proposition. 3 If a small error θ is done on the estimated normal, a 2-jet interpolation give the Gauss curvature with a linear error wrt θ :

$$k_Q - k_S = \theta O(h^{-1}) + O(h) + O(\theta^2).$$

For a fixed h , the curvature error is a linear function of the angle between the normals. The term $\theta O(h^{-1})$ shows that if θ is fixed, the smaller h the worse the accuracy. Hence estimating the normal deserves specific care.

4. Plane Curves

All the results proved for surfaces in the previous section can also be proved for curve, and we omit them. Instead, for the interpolation case, we prove an error bound between the coefficients of the curve and those of the jet.

4.1. Problem addressed

Let C be a curve, and consider the height function f following Equation (1) in any coordinate system whose y axis is not tangent to the curve and, whose origin is on the curve (this implies that $B_0 = 0$). We shall fit C by a n -jet $J_{A,n}(x)$ whose graph is denoted Q . As already mentioned, there are $n + 1$ unknown coefficients A_i s, we assume N data points $P_i(x_i = a_i h, y_i)$ are given, where $N = n + 1$ for interpolation fitting and, $N > n + 1$ for approximation. Notice again that parameter h specifies the uniform convergence of these data points to the origin. The fitting equations are:

$$y_i = f(x_i) = J_{B,n}(x_i) + O(x_i^{n+1}) = J_{A,n}(x_i).$$

Since curve C is given by Equation (1), the normal and the curvature of C at the origin are given by

$$n_C = (-B_1, 1)^t / \sqrt{1 + B_1^2}, \quad k_C = 2B_2 / (1 + B_1^2)^{3/2}. \quad (13)$$

Moreover, in the Monge coordinate system $-B_1 = 0$, these expressions simplify to $n_C = (0, 1)^t$ and $k_C = 2B_2$.

4.2. Error bounds for the interpolation

The equivalent of Prop. 1 for curves gives the magnitude of the accuracy of the interpolation. We can actually be more precise and provide precise error bounds depending upon the function interpolated as well as the relative position of the sample points used.

Proposition. 4 Consider a degree n ($n \geq 2$) interpolation problem for a curve $y = f(x)$. Let ϵ be a positive number so that the interpolation point abscissa lie in the interval $[-\epsilon, \epsilon]$. Let c be a positive constant so that $\sup_{x \in [-\epsilon, \epsilon]} |f^{(n+1)}(x)| \leq c$. At last, let $d \leq 1$ be defined by $\min_{i \neq j} |x_i - x_j| = 2\epsilon d / n$. (d is a measure of the minimum distance between the interpolation points.) Then for $k = 0, \dots, n$:

$$|A_k - B_k| \leq \epsilon^{(n-k+1)} c \left(\frac{n}{2d} \right)^{\frac{n(n-1)}{2}}.$$

Here is an application of the previous result. Let θ denote the angle between the normal and the estimated normal. We have $\sin(\theta) = \|n_Q \wedge n_C\| = |A_1 - B_1| / \sqrt{(1 + A_1^2)(1 + B_1^2)} \leq |A_1 - B_1|$. It is found that

$$\theta \leq \arcsin(\epsilon^n c \left(\frac{n}{2d} \right)^{\frac{n(n+1)}{2}}).$$

Therefore, the coordinate system minimizing the error in the worst case is the one with respect to which the pairwise differences between the abscissa of the sample points is maximized. Generalizing this result for the curvature involves cumbersome calculations.

5. Algorithm

The fitting algorithm to estimate the differential properties at a point p consists of (i)collecting the points used for the fitting. Recall that a n -jet involves $N_n = (n + 1)(n + 2)/2$ coefficients, so that when interpolating (approximating) we assume $N = N_n$ ($N > N_n$). (ii)solving the linear system (iii)recovering the differential properties. We examine in turn the details of these three steps.

5.1. Collecting N neighbors

The mesh case. Although no topological information is required by the fitting method, the connectivity information of a mesh can be used as follows. We sequentially visit the one-ring neighbors, two-ring neighbors, and so on until N points have been collected. Let R_1, \dots, R_k be the k rings of neighbors necessary to collect N neighbors. All the points of the $k - 1$ first rings are used. The complement up to N points is chosen arbitrarily out of the k th ring.

The point-cloud case. The normal at p is first estimated, and the neighbors of p are further retrieved from a power diagram in the estimated tangent plane ³—a provably good procedure if the samples are dense enough. If the number of

neighbors collected is less than N , we recursively collect the neighbors of the neighbors.

Collecting the points therefore boils down to estimating the tangent plane. One solution is to construct the Voronoi diagram of the point set and use these Voronoi vertices called *poles*^{1,11}. Poles yield an accurate estimate of the normal vector but require a global construction.

An alternative is to resort to the algorithm of section 3, and solve a degree one interpolation problem—which requires three points and is well poised as soon as the three points are not collinear. Geometrically, the closer the three points to being aligned, the more unstable the tangent plane estimate. To see how one can get around this difficulty, denote q the nearest neighbor of p . Also, let r be the sample point so that the circum-radius r_{circ} of the triangle pqr is minimum. The estimated normal at p is the normal to the plane through pqr . Intuitively, minimizing the circum-radius r_{circ} prevents two difficulties: on one hand triangles with a large angle (near to π) exhibit a large circum-circle and are discarded; on the other hand, triangles involving a third point r which is not a *local* neighbor of p cannot minimize r_{circ} and are also discarded. A more formal argument advocating the choice of the triangle with minimum r_{circ} is provided in³⁰, where it is shown that the worst error on the approximation of the gradient of a bivariate function by a linear interpolant precisely involves r_{circ} .

5.2. Solving the fitting problem

The next stage consists of choosing the z direction to work with. Since the tangent plane has not been estimated, we use a principal component analysis to compute a rough estimate of the normal with the neighboring points. The polynomial fitting can be done in any coordinate system whose z axis is not tangent to the surface. Hence at least one of the three axis of the world coordinate system matches this requirement. A natural choice is to select the coordinate axis whose angle with the rough estimated normal is minimum. For these coordinates, we fill the Vandermonde matrix. The matrix is further scaled as explained in section 2.3, with h the average value of the norms $\|(x_i, y_i)\|$. The corresponding system is solved using a Singular Value Decomposition. Practically, we use the SVD of the Gnu Scientific Library, available from <http://sources.redhat.com/gsl>.

As pointed out in section 2.3, the instability of the system is provided by the condition number. Whenever degenerate configurations are detected, one can proceed as follows. For the approximation strategy, one can either keep the same degree and increase the number of points used, or reuse the same points with a lower degree. These changes are likely to provide a non singular matrix M . In the worst-case, a degree one fitting must be possible since then only three linearly independent points are required! For the interpolation, things are a bit more involved since reducing the interpolation degree requires discarding some points. Selecting the subset

yielding the best conditioning is a challenging problem^{20,17}. Notice also that for the approximation case, one can always retrieve a solution from an under-constrained least-square problem by choosing, e.g., the solution vector of least norm.

5.3. Retrieving differential quantities

We have already mentioned how to compute the normal. For the second order information, we compute the Weingarten map of the surface¹⁰Section 3.3. Its eigenvalues (eigenvectors) provide the principal curvatures (directions) of the surface. For a parameterized surface given as a height function, one ends up with the formula given on Table 1. Notice that a basis of the tangent space associated to the parameterization $X(u, v) = (u, v, h(u, v))$ consists of the two vectors $X_u = (1, 0, h_u)^t$ and $X_v = (0, 1, h_v)^t$. A Gram-Schmidt orthonormalization of the basis $\{X_u, X_v\}$ gives another basis $\{Y, Z\}$ of the tangent space. The diagonalization of the symmetric matrix representing the Weingarten map in the basis $\{Y, Z\}$ provides the expression of the principal curvature directions with respect to the $\{Y, Z\}$ orthonormal basis. Note that the sign of principal curvatures and hence the definition of minimal and maximal directions rely on the orientation of the normal. As long as our experimental study is performed on meshes of oriented surfaces, it is straightforward to find a global and coherent orientation of the normals.

$$\begin{aligned} E &= 1 + a_1^2 & e &= \frac{2a_3}{\sqrt{a_1^2 + 1 + a_2^2}} \\ F &= a_2 a_1 & f &= \frac{a_4}{\sqrt{a_1^2 + 1 + a_2^2}} \\ G &= 1 + a_2^2 & g &= \frac{2a_5}{\sqrt{a_1^2 + 1 + a_2^2}} \end{aligned} \quad A^t = - \begin{pmatrix} e & f \\ f & g \end{pmatrix} \begin{pmatrix} E & F \\ F & G \end{pmatrix}^{-1}$$

Table 1: Computing the matrix A of the Weingarten map of $h(u, v) = a_1 u + a_2 v + a_3 u^2 + a_4 uv + a_5 v^2$ in the basis $\{X_u, X_v\}$

6. Experimental study

We present results along two lines. First, we illustrate the convergence theorems proved in section 3. Second, we present illustrations on standard computer graphics models.

6.1. Convergence estimates on a graph

Setup. We illustrate the convergence properties with the smooth height field $f(u, v) = 0.1e^{2u+v-v^2}$ defined over the parametric domain $(u, v) \in [-0.5, 0.5]^2$ —see Figs. 4. At selected points on the graph of f , we study the angle between the normals—more precisely its sine $\sin(n, \bar{n})$, and the relative errors on principal curvatures. The values output by our algorithm are compared against the exact values computed analytically with arbitrary precision under Maple, and we report both average and maximum errors over samples points. More precisely, the graph of f is sampled with points

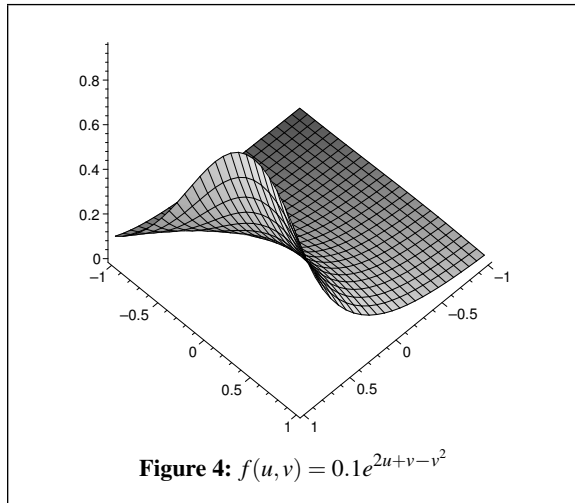
$p_i(x_i, y_i, f(x_i, y_i))$ where the (x_i, y_i) s lies on a randomly perturbed triangulated square grid of side h . The triangulation is randomly perturbed to avoid simple degenerate configurations such as points lying on lines. The perturbation for the point (u, v) of the regular grid is the point (x, y) with $x = u + \delta h$, $y = v + \delta' h$ and δ, δ' random numbers in $[0, 0.9]$. The connectivity of the graph is that of the triangulated grid.

The convergence properties are illustrated (i) with respect to the discretization step h of the grid —for a given fitting degree n (ii) with respect to the fitting degree n —for a given discretization step h . We compare the convergence properties of the interpolation and approximation schemes, for fitting degrees ranging from one to nine. To quantify the observations, notice that according to theorem 3, the error δ on a k^{th} -order differential quantity is $O(h^{n-k+1})$, hence

$$\delta \approx c h^{n-k+1} \Leftrightarrow \log(1/\delta) \approx \log(1/c) + (n - k + 1) \log(1/h) \tag{14}$$

$$\Leftrightarrow \frac{\log(1/\delta)}{\log(1/h)} \approx \frac{\log(1/c)}{\log(1/h)} + (n - k + 1). \tag{15}$$

Figures 5 to 12 illustrate the convergence behaviour —see 6 for enlarged versions.



Convergence wrt to h . To highlight the convergence properties with respect to the size of the neighborhood, we consider sequences of meshes with $h \rightarrow 0$, more precisely h ranges from 2^{-2} to 2^{-6} .

Curves of Figs. 5 to 10 show the average convergence behavior as the size of the neighborhood decreases. For a given degree and following equation (14), curves of figures 5 to 10 should be lines of slope $(n - k + 1)$. The behavior is more regular for the approximation case, and the estimate is also better: a gain of about a digit can be observed between k_{max} estimates of figures 9 and 10.

Convergence wrt to the fitted polynomial degree.

Curves of figures 11 and 12 show the convergence as a function of the degree of the fitted polynomial for a fixed neighborhood size. According to Eq. (15), curves of these figures should be lines of unit slope, with a vertical shift of one unit between normal and curvatures errors since curvature is a 2^{nd} order quantity whereas normal is 1^{st} order. The gap between the average values and the maximal values is greater for interpolation than for approximation. The particular case of a degree 7 approximation reveals to be worse than expected, due to the regular connectivity of the mesh used to find the neighbors: there is only one more point than for the degree 7 interpolation fitting. Other charts providing the conditioning and the least singular value can be found in 6. Interpolation fitting is always more ill-conditioned than approximation, and closer to a degenerate problem (the least singular value is the distance of the matrix system to singular matrices).

6.2. Illustrations (see color section)

We depict differential informations on several models. When principal directions are displayed, blue and red respectively correspond to k_{min} and k_{max} —that is $k_{min} \leq k_{max}$ —, assuming the surface normal points to the outside. To display patches of osculating n -jets, it is sufficient to select a rectangular domain in parameter space, sample it with a grid, and plot the corresponding mesh.

Consider the mesh models of the elliptic paraboloid $z = 2x^2 + y^2$ —16k points, Fig. 1—, and the surface of revolution $z = 0.1 \sin(10\sqrt{(x^2 + y^2)})$ —8k points, Fig. 2. The arrangement of curvature lines provides informations on umbilical points —where principal directions are not defined since $k_{min} = k_{max}$. On the paraboloid, it is easy to follow curvature lines and see how they turn around an umbilic. The surface of revolution provides an example of two parabolic lines (where the principal curvature k_{max} vanishes), that is a curve along which the Gauss curvature K_{Gauss} vanishes. This specific line splits the surface into elliptic ($K_{Gauss} > 0$) and hyperbolic regions ($K_{Gauss} < 0$). This model also illustrates a line of umbilical points where minimum and maximum principal directions swap each over.

For a standard example from Computer Graphics, consider the Michelangelo’s David of Fig. 3. On this model of 95922 pts, the principal curvatures provide meaningful information for shape perception (See also 18p197 as well as 15.) To finish up, we illustrate the robustness of the method. Figure 4 displays random patches on the Mechanic model, a 12,500 points model reconstructed from the output of a range scanner. In spite of the coarse sampling, patches and principal directions provide faithful information. In a similar vein, approximation fitting with large neighborhoods Fig. 5 features a noisy triangulation of a graph. In spite of the severe level of noise, surface patches *average* the available information. On Fig. 6, a noisy triangulation of an ellipsoid, 15k

points, principal directions are enough precise to recognize an umbilic.

7. Conclusion

Estimating differential quantities is of prime importance in many applications from Computer Vision, Computer Graphics, Computer Aided Design or Computational Geometry. This importance accounts for the many different differential estimators one can find in the vast literature of applied geometry. Unfortunately, few of these have undergone a precise theoretical analysis. Another striking fact is that estimates of second order differential quantities are always computed using degenerate conics/quadratics without even mentioning the classification of Euclidean conics/quadratics.

The main contribution of the paper is to bridge the gap between the question of estimating differential properties of arbitrary order and multivariate interpolation and approximation. In making this connection, the use of jets—truncated Taylor expansions—is advocated. Precise asymptotic convergence rates are proved for curves and surfaces, both for the interpolation and approximation schemes. To the best of our knowledge, these results are among the first ones providing accurate estimates for differential quantities of order three and more. Experimental results for surfaces of \mathbb{R}^3 are reported. These experiments illustrate the asymptotic convergence results, but also the robustness of the methods on general Computer Graphics models.

References

1. Nina Amenta and Marshall Bern. Surface reconstruction by Voronoi filtering. *Discrete Comput. Geom.*, 22(4):481–504, 1999.
2. M. Berger. *Geometry (vols. 1-2)*. Springer-Verlag, 1987.
3. J.-D. Boissonnat and J. Flototto. A local coordinate system on a surface. In *ACM symposium on Solid modeling*, Saarbrücken, 2002.
4. V. Borrelli, F. Cazals, and J.-M. Morvan. On the angular defect of triangulations and the pointwise approximation of curvatures. In *Curves and Surfaces*, St Malo, France, 2002. INRIA Research Report RR-4590.
5. J.W. Bruce and P.J. Giblin. *Curves and singularities (2nd Ed.)*. Cambridge, 1992.
6. F. Cazals and M. Pouget. Estimating differential quantities using polynomial fitting of osculation jets. Research Report RR-4823, INRIA Sophia Antipolis, 2003.
7. C. Coatmelec. Approximation et interpolation des fonctions différentielles de plusieurs variables. *Ann. Sci. Ecole Norm. Sup.*, 83, 1966.
8. D. Cohen-Steiner and J.-M. Morvan. Restricted delaunay triangulations and normal cycle. In *ACM Symposium on Computational Geometry*, 2003.
9. P. Csàkány and A.M. Wallace. Computation of local differential parameters on irregular meshes. In Springer, editor, *Mathematics of Surfaces*. R. Cipolla and R. Martin Eds, 2000.
10. M. do Carmo. *Differential Geometry of Curves and Surfaces*. Prentice-Hall, 1976.
11. S. Funke and E. A. Ramos. Smooth-surface reconstruction in near-linear time. In *ACM SODA'02*, 2002.
12. M. Gasca and T. Sauer. Polynomial interpolation in several variables. *Advances in Comp. Math.*, 12(4), 2000.
13. J. Goldfeather. Understanding errors in approximating principal direction vectors. Technical Report 01-006, University of Minnesota, Computer Science and Engineering, 2001.
14. G. Golub and C. van Loan. *Matrix Computations*. Johns Hopkins Univ. Press, Baltimore, MA, 1983.
15. P. W. Hallinan, G. Gordon, A.L. Yuille, P. Giblin, and D. Mumford. *Two-and Three-Dimensional Patterns of the Face*. A.K.Peters, 1999.
16. P.W. Hallinan et al. *Two and Three-Dimensional Patterns of the Face*. A.K. Peters, 1999.
17. N.J. Higham. *Accuracy and Stability of Numerical Algorithms*. SIAM, 1996.
18. D. Hilbert and S. Cohn-Vossen. *Geometry and the Imagination*. Chelsea, 1952.
19. P. Lancaster and K. Salkauskas. *Curve and surface fitting: an introduction*. Academic, 1986.
20. M. Lassak. Parallelotopes of maximum volumes in a simplex. *Disc. Comp. Geometry*, 21, 1999.
21. D. Levin. Mesh-independent surface interpolation. *Geometric Modeling for Scientific Visualization*, 2003.
22. D. Meek and D. Walton. On surface normal and Gaussian curvature approximations given data sampled from a smooth surface. *Computer-Aided Geometric Design*, 17:521–543, 2000.
23. J.-M. Morvan and B. Thibert. Smooth surface and triangular mesh : Comparison of the area, the normals and the unfolding. In *ACM Symposium on Solid Modeling and Applications*, 2001.
24. S. Petitjean. A survey of methods for recovering quadratics in triangle meshes. *ACM Computing Surveys*, 34(2), 2001.
25. K. Polthier and M. Schmies. Straightest geodesics on polyhedral surfaces. In *Mathematical Visualization*, H.C. Hege, K. Polthier Editors, 1998.

26. I. Porteous. *Geometric Differentiation (2nd Edition)*. Cambridge University Press, 2001.
27. P. Sander and S. Zucker. Inferring surface trace and differential structure from 3-D images. *IEEE Trans. Pattern Analysis and Machine Intelligence*, 12(9):833–854, 1990.
28. T. Sauer. Computational aspects of multivariate polynomial interpolation. *Advances in Comp. Math.*, 3(3), 1995.
29. T. Sauer and Yuan Xu. On multivariate lagrange interpolation. *Math. Comp.*, 64, 1995.
30. Jonathan R. Shewchuk. What is a good linear element? interpolation, conditioning, and quality measures. In *11th International Meshing Roundtable*, Ithaca, New York, USA, 2002.
31. M. Spivak. *A comprehensive introduction to Differential Geometry (Third Ed.)*. Publish or Perish, 1999.
32. G. Taubin. Estimating the tensor of curvature of a surface from a polyhedral approximation. In *Fifth International Conference on Computer Vision*, 1995.
33. K. Watanabe and A.G. Belyaev. Detection of salient curvature features on polygonal surfaces. In *Eurographics*, 2001.

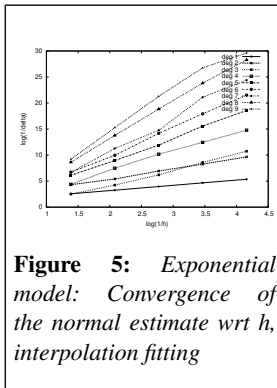


Figure 5: Exponential model: Convergence of the normal estimate wrt h , interpolation fitting

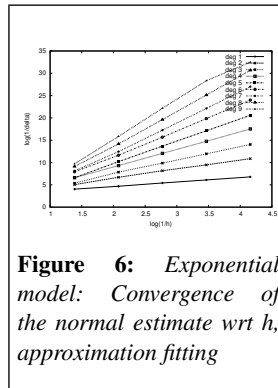


Figure 6: Exponential model: Convergence of the normal estimate wrt h , approximation fitting

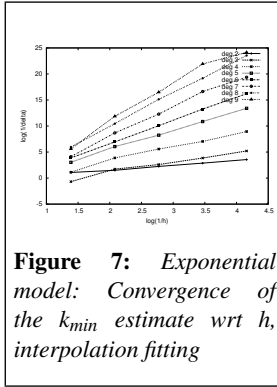


Figure 7: Exponential model: Convergence of the k_{min} estimate wrt h , interpolation fitting

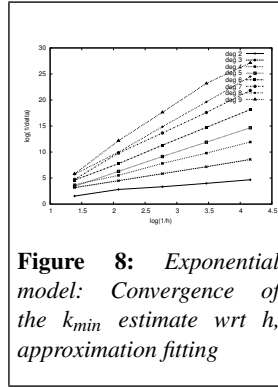


Figure 8: Exponential model: Convergence of the k_{min} estimate wrt h , approximation fitting

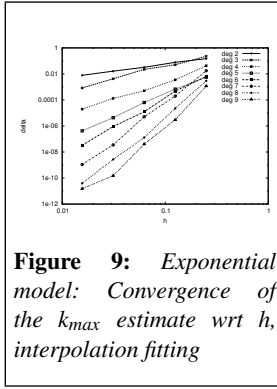


Figure 9: Exponential model: Convergence of the k_{max} estimate wrt h , interpolation fitting

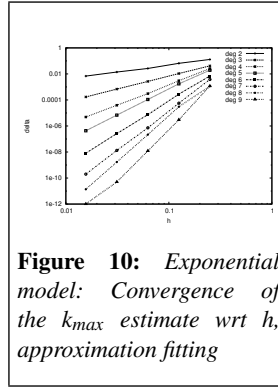


Figure 10: Exponential model: Convergence of the k_{max} estimate wrt h , approximation fitting

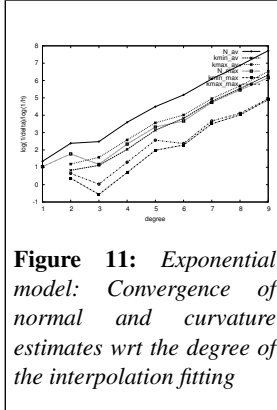


Figure 11: Exponential model: Convergence of normal and curvature estimates wrt the degree of the interpolation fitting

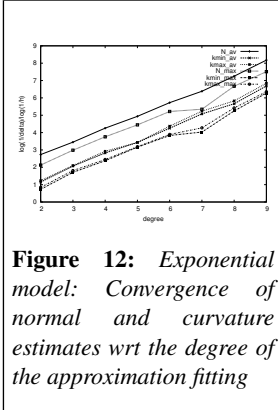


Figure 12: Exponential model: Convergence of normal and curvature estimates wrt the degree of the approximation fitting